



Deposited via The University of Leeds.

White Rose Research Online URL for this paper:

<https://eprints.whiterose.ac.uk/id/eprint/81061/>

Version: Accepted Version

Article:

Karageorghis, A, Lesnic, D and Marin, L (2014) Regularized collocation Trefftz method for void detection in two-dimensional steady-state heat conduction problems. *Inverse Problems in Science and Engineering*, 22 (3). 395 - 418. ISSN: 1741-5977

<https://doi.org/10.1080/17415977.2013.788172>

Reuse

Items deposited in White Rose Research Online are protected by copyright, with all rights reserved unless indicated otherwise. They may be downloaded and/or printed for private study, or other acts as permitted by national copyright laws. The publisher or other rights holders may allow further reproduction and re-use of the full text version. This is indicated by the licence information on the White Rose Research Online record for the item.

Takedown

If you consider content in White Rose Research Online to be in breach of UK law, please notify us by emailing eprints@whiterose.ac.uk including the URL of the record and the reason for the withdrawal request.

REGULARIZED TREFFTZ COLLOCATION METHOD FOR VOID DETECTION IN TWO-DIMENSIONAL STEADY-STATE HEAT CONDUCTION PROBLEMS

A. KARAGEORGHIS, D. LESNIC, AND L. MARIN

ABSTRACT. We propose the use of the Trefftz collocation method for the solution of inverse geometric problems and, in particular, the determination of the boundary of a void. As was the case in the solution of such problems using the method of fundamental solutions, the algorithm for imaging the interior of the medium also makes use of radial polar parametrization of the unknown void shape in two dimensions. The centre of this radial polar parametrization is considered to be unknown. The feasibility of this new method is illustrated by several numerical examples highlighting its advantages and shortcomings.

1. INTRODUCTION

Numerous practical problems in engineering and sciences are characterised by the fact that one or more of the following conditions are partially or entirely unknown: the geometry of the domain of interest, the complete boundary and initial conditions, the material properties and the external sources acting in the solution domain. These problems are known as *inverse problems* and it are, in general, ill-posed [18], in the sense that the existence, uniqueness and stability of their solutions are not always guaranteed, and hence more difficult to solve. An important class of inverse problems is represented by the so-called *inverse geometric problems* whose main feature is the lack of knowledge of part of the boundary. In particular, we focus herein on the numerical reconstruction of an internal boundary (i.e. cavity or rigid inclusion) in steady-state isotropic heat conduction (Laplace's equation) from the knowledge of the temperature and normal heat flux (i.e. Cauchy data) on the outer boundary and an appropriate boundary condition for the unknown void.

The uniqueness of solution of the inverse geometric steady-state heat conduction problem related to the determination of rigid inclusions or cavities from Cauchy data prescribed on the outer boundary of the solution domain for media with constant conductivity was proved in [19] and [48], respectively. The numerical reconstruction of voids in heat conduction problems has been tackled by numerous authors and various approaches have been proposed for the solution of this inverse geometric problem, see e.g. [1, 6, 13, 17, 27, 28, 32, 33, 34, 35, 46, 47, 53]. Das and Mitra [13] developed an iterative algorithm to determine the location and shape of a flaw in steady-state heat conduction (i.e. Laplace's equation). Kassab and Pollard [32, 33] proposed a linear boundary element method (BEM), an anchored grid pattern method and a Newton-Raphson method with a Broyden update for the numerical reconstruction of an unknown cavity for the same inverse geometric heat conduction problem. The conjugate gradient method (CGM) for the numerical solution of inverse design problems in estimating the optimal locations and shapes of the internal cooling passages for turbine blades based on the desired outer surface temperature distribution was considered in [24]. Gallego and Suarez [17] proposed an approach based on a boundary integral equation for the variation of the potential and flux to retrieve numerically an assumed flaw in the case of a two-dimensional isotropic solid subject to thermal loads. An iterative algorithm based on a real coded genetic algorithm (GA) and the BEM for detecting cavities in problems governed by the two-dimensional Laplace equation was developed in [46], while [6] proposed a simplification of the CGM for the reconstruction of voids in two-dimensional steady-state isotropic heat conduction which consists of prescribing the values of the step size for the optimal searches to be constant values

Date: November 5, 2012.

2000 Mathematics Subject Classification. Primary 65N35; Secondary 65N21, 65N38.

Key words and phrases. Void detection, inverse problem, Trefftz method, collocation.

depending upon the resolution of the identification. An iterative algorithm using thermographic techniques based on the superposition of clusters of sources/sinks with the BEM [34] was employed for the detection of subsurface cavities and flaws. Mera [47] used kriging approximation models to speed-up the optimization process via GAs for detecting the size and location of subsurface cavities associated with the two-dimensional Laplace's equation, whilst Tan et al. [50] solved a geometry identification problem in two-dimensional isotropic heat conduction by employing the least-squares collocation meshless method and CGM. Kazemzadeh-Parsi and Daneshmand [35] approached the cavity detection problem for the two-dimensional Laplace equation via the smoothed fixed grid finite element method in conjunction with the CGM. Yan and Ma [53] considered the reconstruction of a cavity in the case of the Laplace equation from the knowledge of the measurements on the exterior boundary and employed the domain derivative of the associated operator and a regularized Newton method for the solution of the corresponding ill-posed and nonlinear problem. Recently, Karageorghis and Lesnic [27] proposed a method of fundamental solution (MFS)-based reconstruction of a cavity for the two-dimensional stationary heat conduction equation in isotropic media, whereas Borman et al. [1] and Karageorghis and Lesnic [28] employed the same approach for the detection of inclusions.

Trefftz methods [51] have been used extensively for the solution of elliptic boundary value problems, see, for example [38, 39, 52], and also [55]. Surveys on Trefftz and related methods may be found in [26, 36, 40, 55]. In this work we investigate the performance of the Trefftz collocation method (TCM) for the solution of inverse geometric problems, in particular for void detection problems. The TCM is a boundary meshless method and such methods have, in recent years, become increasingly popular for the solution of inverse problems in general because of the ease with which they can be implemented for boundary value problems in complex geometries and in three dimensions. The MFS in particular has been used extensively for the solution of inverse problems [30]. Trefftz methods have been used for the solution of inverse Cauchy linear problems [7, 8, 9, 10, 31, 43, 54]. In the case of inverse geometric problems the TCM has been recently used by Fan and his co-workers [3, 14, 15]. In particular, [15] deals entirely with boundary identification problems for Laplace's equation, while in [3] an internal void problem is solved in the case of the Helmholtz equation. The ideas developed in this work are close to the ones developed in [14], see also [2], where two internal void detection problems are solved in the case of the Laplace equation. However, our proposed algorithm differs from the one in [14] as follows:

- In contrast to the algorithm of [14] for void detection inverse problems, we consider problems in which the centre(s) of the void(s) to be reconstructed is (are) unknown. The coordinates of the centre(s) are merely taken as additional unknowns in the algorithm.
- By changing and augmenting the Trefftz basis, the algorithm is capable of locating multiple inclusion with unknown centres.
- Instead of using a scalar homotopy algorithm we use the state-of-the-art `MATLAB` optimization toolbox routine `lsqnonlin`. This routine allows for the imposition of simple bounds on the variable which, to a great extent, eliminates physically unrealistic solutions.
- The stability of the proposed algorithm is achieved using two regularization parameters which can be determined by the use of the L-curve criterion. The method is shown to accurately reconstruct smooth or piecewise smooth, convex or concave, single or multiple cavities and rigid inclusions.
- We are not using the so-called modified collocation Trefftz method of [41, 42] which takes into account the characteristic shapes of the domains involved. This is because the size of at least one of the domains is unknown and needs to be determined as part of the solution. Efforts to normalize one set of unknowns produced little or no difference to our results.

In comparison to the MFS, the TCM does not require selecting a fictitious boundary curve on which source points need to be positioned. However, a disadvantage of the TCM with respect to the MFS is the poor conditioning of the discretization matrices [42, 56] and we aim to also address this issue in the application of the TCM to void detection problems. In fact, the connection between the TCM and the MFS has recently been pointed out in [5] where it is shown that for the Laplace equation in a bounded, simply-connected domain the TCM is retrieved as

a degenerate situation of the MFS with the source points placed at infinity. The corresponding result in annular and exterior domains may be found in [4] and [49], respectively.

2. MATHEMATICAL FORMULATION

In this section we formulate the direct and inverse problems related to a void such as a rigid inclusion or a cavity in the case of steady-state heat conduction (Laplace's equation). The direct problem given by the Laplace equation

$$\Delta u = 0 \quad \text{in } \Omega, \quad (2.1a)$$

subject to the Dirichlet boundary condition

$$u = f \quad \text{on } \partial\Omega_2, \quad (2.1b)$$

and the homogeneous boundary condition

$$\alpha u + (1 - \alpha)\partial_n u = 0 \quad \text{on } \partial\Omega_1, \quad \text{where } \alpha \in \{0, 1\}, \quad (2.1c)$$

has a unique weak solution $u \in \mathcal{H}^1(\Omega)$ if $f \in \mathcal{H}^{1/2}(\partial\Omega_2)$, and a unique classical solution $u \in \mathcal{C}^2(\Omega) \cap \mathcal{C}(\bar{\Omega})$, provided f is sufficiently smooth. In the above, $\Omega = \Omega_2 \setminus \Omega_1$, where $\bar{\Omega}_1 \subset \Omega_2$, is a bounded annular domain with boundary $\partial\Omega = \partial\Omega_1 \cup \partial\Omega_2$ and we assume that Ω is connected. Equation (2.1c), covers both Dirichlet ($\alpha = 1$), i.e. a rigid inclusion, and Neumann ($\alpha = 0$), i.e. a cavity, boundary conditions on $\partial\Omega_1$.

The inverse problem we are concerned with consists of determining not only the function u , but also the void Ω_1 so that u satisfies the Laplace equation (2.1a), given the Dirichlet data $f \neq \text{constant}$ in (2.1b), the homogeneous boundary condition (2.1c) and the Neumann current flux measurement

$$g := \partial_n u \quad \text{on } \partial\Omega_2. \quad (2.1d)$$

In (2.1c) and (2.1d), the vector \mathbf{n} denotes the outward unit normal to the annular domain Ω .

When $\alpha = 0$, for (2.1a), (2.1c) and (2.1d) to be consistent, we require

$$\int_{\partial\Omega_2} g(s) ds = 0. \quad (2.2)$$

In contrast to the direct (forward) boundary value problem (2.1a)-(2.1c), the inverse problem (2.1a)-(2.1d) is nonlinear and ill-posed. Although the solution is unique, [19], it is unstable with respect to small errors in the input Cauchy data (2.1b) and (2.1d).

3. TREFFTZ COLLOCATION METHOD

In the TCM for the doubly-connected two-dimensional annular domain Ω , we seek an approximation to the solution of Laplace's equation (2.1a) as a linear combination of T-complete functions in the form [42, 22, 23]

$$\begin{aligned} u_N(\boldsymbol{\alpha}, \boldsymbol{\beta}, \boldsymbol{\gamma}, \boldsymbol{\delta}; \mathbf{x}) &= \alpha_0 + \gamma_0 \log |z| + \sum_{k=1}^N \alpha_k \Re \{z^k\} + \sum_{k=1}^N \beta_k \Im \{z^k\} \\ &+ \sum_{k=1}^N c_k \Re \{z^{-k}\} + \sum_{k=1}^N d_k \Im \{z^{-k}\}, \quad \mathbf{x} = (x, y) \in \bar{\Omega}, \end{aligned} \quad (3.1)$$

where the T-complete system is given by

$$\{1, \log |z|, \Re(z^n), \Im(z^k), \Re(z^{-k}), \Im(z^{-k}); z = x + iy, k \in \mathbb{N}\}, \quad (3.2)$$

where \Re and \Im denote the real and imaginary part of a complex number, respectively. In (3.1), there are $4N + 2$ unknowns, namely the coefficients $\boldsymbol{\alpha} = [\alpha_0, \alpha_1, \dots, \alpha_N]^T$, $\boldsymbol{\beta} = [\beta_1, \beta_2, \dots, \beta_N]^T$, $\boldsymbol{\gamma} = [\gamma_0, \gamma_1, \dots, \gamma_N]^T$, $\boldsymbol{\delta} = [\delta_1, \delta_2, \dots, \delta_N]^T$.

Without loss of generality, we shall assume that the (known) fixed exterior boundary $\partial\Omega_2$ is a circle of radius R . As a result, the outer boundary collocation points are chosen as

$$\mathbf{x}_{M_1+\ell} = R(\cos \tilde{\vartheta}_\ell, \sin \tilde{\vartheta}_\ell), \quad \ell = \overline{1, M_2}, \quad (3.3)$$

where $\tilde{\vartheta}_\ell = \frac{2\pi(\ell-1)}{M_2}$, $\ell = \overline{1, M_2}$.

We further assume that the unknown boundary $\partial\Omega_1$ is a smooth, star-like curve with respect to the centre which has unknown coordinates (X, Y) . This means that its equation in polar coordinates can be written as

$$x = X + r(\vartheta) \cos \vartheta, \quad y = Y + r(\vartheta) \sin \vartheta, \quad \vartheta \in [0, 2\pi), \quad (3.4)$$

where r is a smooth 2π -periodic function. The constraint that $\Omega_1 \subset \Omega_2$ then recasts as

$$(X + r(\vartheta) \cos \vartheta)^2 + (Y + r(\vartheta) \sin \vartheta)^2 < R^2, \quad \vartheta \in [0, 2\pi). \quad (3.5)$$

The discretized form of (3.4) for $\partial\Omega_1$ becomes

$$r_k = r(\vartheta_k), \quad k = \overline{1, M_1} \quad (3.6)$$

and we choose the inner boundary collocation points as

$$\mathbf{x}_k = (X, Y) + r_k (\cos \vartheta_k, \sin \vartheta_k), \quad (3.7)$$

where $\vartheta_k = \frac{2\pi(k-1)}{M_1}$, $k = \overline{1, M_1}$.

Since the centre is not known and therefore not necessarily the origin, the basis (3.2) needs to be modified to

$$\{1, \log |z - z_0|, \Re(z^n), \Im(z^n), \Re((z - z_0)^{-n}), \Im((z - z_0)^{-n}); z = x + iy, n \in \mathbb{N}\}, \quad (3.8)$$

where $z_0 = X + iY$. For example, this is suggested by function theoretic results concerning the expansion of functions that are analytic in multiply-connected domains [16, page 244], see also [37]. Therefore, the TCM approximation becomes

$$\begin{aligned} u_N(\boldsymbol{\alpha}, \boldsymbol{\beta}, \boldsymbol{\gamma}, \boldsymbol{\delta}; \mathbf{x}) &= \alpha_0 + \gamma_0 \log |z - z_0| + \sum_{k=1}^N \alpha_k \Re\{z^k\} + \sum_{k=1}^N \beta_k \Im\{z^k\} \\ &+ \sum_{k=1}^N \gamma_k \Re\{(z - z_0)^{-k}\} + \sum_{k=1}^N \delta_k \Im\{(z - z_0)^{-k}\}, \quad \mathbf{x} = (x, y) \in \bar{\Omega}. \end{aligned} \quad (3.9)$$

In the cases where $R > 1$ we tried to scale the terms in the first and second series in (3.9) through division with R^k as suggested by Liu [41, 42]. This produced little or no improvement to our results. This may be because the corresponding multiplication of each of the terms in the third and fourth series in (3.9) by R_c^k , where R_c is the characteristic length of $\partial\Omega_1$, as suggested in [42] is not possible as its size is unknown.

4. IMPLEMENTATIONAL DETAILS

The current flux data (2.1d) come from practical measurements which is inherently contaminated with errors due to noise, and we therefore replace g by the noisy data g^ε defined as

$$g^\varepsilon(\mathbf{x}_j) = (1 + \rho_j p) g(\mathbf{x}_j), \quad j = \overline{M_1 + 1, M_1 + M_2}, \quad (4.1)$$

where p represents the percentage of noise and ρ_j is a pseudo-random noisy variable drawn from a uniform distribution in $[-1, 1]$ using the MATLAB command `-1+2*rand(1, M2)`. It is also reported that in our numerical experiments we observed that the effect of noise added to the Dirichlet boundary data (2.1b) was similar to that of perturbing the Neumann data. As a result in the numerical results section we only present results for the noisy Neumann data (4.1).

The coefficients $(a_k)_{k=0,\overline{N}}$, $(b_k)_{k=0,\overline{N}}$, $(c_k)_{k=1,\overline{N}}$ and $(d_k)_{k=1,\overline{N}}$ in (3.1), the radii $(r_k)_{k=1,\overline{M_1}}$ in (3.6), and the coordinates of the centre $\mathbf{C} = (X, Y)$ are determined by imposing the boundary conditions (2.1b), (2.1c) and (2.1d) in a least-squares sense. This leads to the minimization of the functional

$$\begin{aligned}
S(\boldsymbol{\alpha}, \boldsymbol{\beta}, \boldsymbol{\gamma}, \boldsymbol{\delta}, \mathbf{r}, \mathbf{C}) : &= \sum_{j=M_1+1}^{M_1+M_2} [u_N(\boldsymbol{\alpha}, \boldsymbol{\beta}, \boldsymbol{\gamma}, \boldsymbol{\delta}; \mathbf{x}_j) - f(\mathbf{x}_j)]^2 + \sum_{j=M_1+1}^{M_1+M_2} [\partial_n u_N(\boldsymbol{\alpha}, \boldsymbol{\beta}, \boldsymbol{\gamma}, \boldsymbol{\delta}; \mathbf{x}_j) - g^\varepsilon(\mathbf{x}_j)]^2 \\
&+ \sum_{j=1}^{M_1} [\alpha u_N(\boldsymbol{\alpha}, \boldsymbol{\beta}, \boldsymbol{\gamma}, \boldsymbol{\delta}; \mathbf{x}_j) + (1 - \alpha) \partial_n u_N(\boldsymbol{\alpha}, \boldsymbol{\beta}, \boldsymbol{\gamma}, \boldsymbol{\delta}; \mathbf{x}_j)]^2 \\
&+ \lambda_1 (|\boldsymbol{\alpha}|^2 + |\boldsymbol{\beta}|^2 + |\boldsymbol{\gamma}|^2 + |\boldsymbol{\delta}|^2) + \lambda_2 \sum_{\ell=2}^{M_1} (r_\ell - r_{\ell-1})^2, \tag{4.2}
\end{aligned}$$

where $\lambda_1, \lambda_2 \geq 0$ are regularization parameters to be prescribed.

In (4.2), the outward normal vector \mathbf{n} is defined as follows:

$$\mathbf{n} = \begin{cases} \cos \vartheta \mathbf{i} + \sin \vartheta \mathbf{j}, & \text{if } \mathbf{x} \in \partial\Omega_2, \\ \frac{1}{\sqrt{r^2(\vartheta) + r'^2(\vartheta)}} [-r'(\vartheta) \sin \vartheta + r(\vartheta) \cos \vartheta] \mathbf{i} + (r'(\vartheta) \cos \vartheta - r(\vartheta) \sin \vartheta) \mathbf{j}, & \text{if } \mathbf{x} \in \partial\Omega_1, \end{cases} \tag{4.3}$$

where $\mathbf{i} = (1, 0)$ and $\mathbf{j} = (0, 1)$. As a result, from (3.9) the normal derivative $\partial_n u_N$ is evaluated as

$$\begin{aligned}
\partial_n u_N &= \mathbf{n} \cdot \nabla u_N = \\
&\mathbf{n} \cdot \left(\gamma_0 \frac{\Re\{z - z_0\}}{|z - z_0|^2} + \sum_{k=1}^N \alpha_k \Re\{kz^{k-1}\} + \sum_{k=1}^N \beta_k \Im\{kz^{k-1}\} \right. \\
&+ \sum_{k=1}^N \gamma_k \Re\{-k(z - z_0)^{-k-1}\} + \sum_{k=1}^N \delta_k \Im\{-k(z - z_0)^{-k-1}\}, \\
&\quad \gamma_0 \frac{\Im\{z - z_0\}}{|z - z_0|^2} + \sum_{k=1}^N \alpha_k \Re\{ikz^{k-1}\} + \sum_{k=1}^N \beta_k \Im\{ikz^{k-1}\} \\
&\left. + \sum_{k=1}^N \gamma_k \Re\{-ki(z - z_0)^{-k-1}\} + \sum_{k=1}^N \delta_k \Im\{-ki(z - z_0)^{-k-1}\} \right). \tag{4.4}
\end{aligned}$$

In (4.3), we use the central finite-difference approximation

$$r'(\vartheta_i) \approx \frac{r_{i+1} - r_{i-1}}{4\pi/M_1}, \quad i = \overline{1, M_1}, \tag{4.5}$$

with the convention that $r_{N+1} = r_1$, $r_0 = r_{M_1}$.

Since the total number of unknowns is $4N + 2 + M_1 + 2$ and the number of boundary condition collocation equations is $M_1 + 2M_2$ we need to take $M_2 \geq 2N + 2$.

4.1. Non-linear minimization. The minimization of functional (4.2) is carried out using the MATLAB [45] optimization toolbox routine `lsqnonlin` which solves nonlinear least squares problems. This routine by default uses the so-called trust-region-reflective algorithm based on the interior-reflective Newton method [11, 12]. In addition, `lsqnonlin` does not require the user to provide the gradient and, in addition, it offers the option of imposing lower and upper bounds on the elements of the vector of unknowns. Further details regarding the application of `lsqnonlin` to inverse geometric problems may be found in [30].

5. NUMERICAL EXAMPLES

5.1. **Example 1.** We first consider an example from the literature for which the exact solution is known [1]. Here we examine the case of a circular rigid inclusion where $\alpha = 1$. In particular, we consider

$$\Omega_1 = \{(x, y) \in \mathbb{R}^2 : x^2 + y^2 < R_0^2 < 1\}, \quad \Omega_2 = \{(x, y) \in \mathbb{R}^2 : x^2 + y^2 < R^2 = 1\} \quad (5.1)$$

and

$$u(x, y) = \log \frac{\sqrt{x^2 + y^2}}{R_0}. \quad (5.2)$$

For any $0 < R_0 < 1$, the function u satisfies problem (2.1a)-(2.1d), with

$$f(x, y) = -\log R_0, \quad g(x, y) = 1, \quad (x, y) \in \partial\Omega_2. \quad (5.3)$$

In our numerical experiments we consider the case $R_0 = 0.5$. We take as initial guesses $\mathbf{r}^0 = \mathbf{0.3}$, $\mathbf{a}^0 = \mathbf{b}^0 = \mathbf{0}$ and $\mathbf{c}^0 = \mathbf{d}^0 = \mathbf{0}$, and we fix as known the centre \mathbf{C} at the origin $(0, 0)$.

In Figure 1 we present the reconstructed curves for various numbers of degrees of freedom obtained in 20 iterations, no noise and no regularization. From this figure it can be seen that very accurate and convergent numerical results are obtained. In Figure 2 we present typical examples of reconstructed curves with noise level of $p = 10\%$ with no regularization and $M_1 = M_2 = 48, N = 8$ for different numbers of iterations. From this figure it can be seen that as the number of iterations increases instabilities start to manifest if no regularization is included. In Figure 3 we present the corresponding reconstructed curves with $p = 10\%$, after 1000 iterations and various regularization parameters λ_1 with $\lambda_2 = 0$. The corresponding curves for various regularization parameters λ_2 with $\lambda_1 = 0$ are presented in Figure 4. In some instances, in this and subsequent examples, the use of regularization leads the iterative process to converge in fewer than the prescribed maximum number of iterations. Overall from Figures 3 and 4 it can be seen that regularization with either $\lambda_1 = 120$ or $\lambda_2 = 1$, respectively, does smooth out the slight oscillations recorded in the results of Figure 2 obtained after 1000 iterations with no regularization.

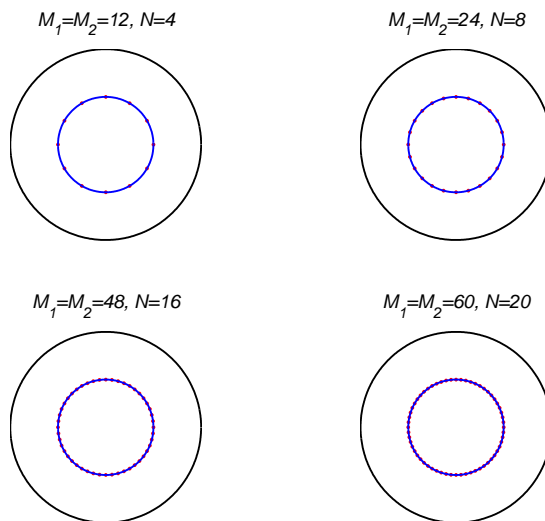


FIGURE 1. Example 1: Results after 20 iteration for various numbers of degrees of freedom, no noise and no regularization.

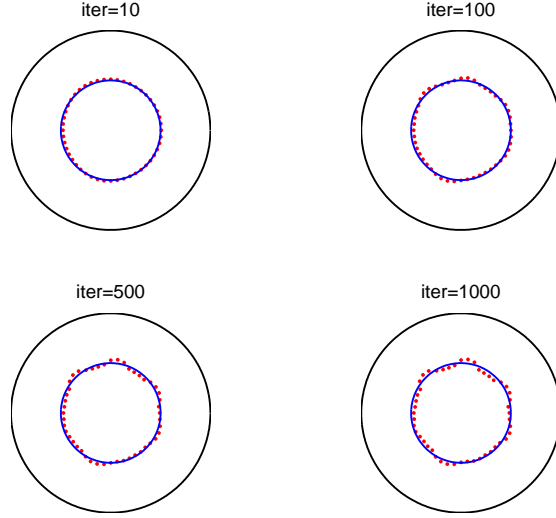


FIGURE 2. Example 1: Results for noise $p = 10\%$, no regularization and various numbers of iterations.

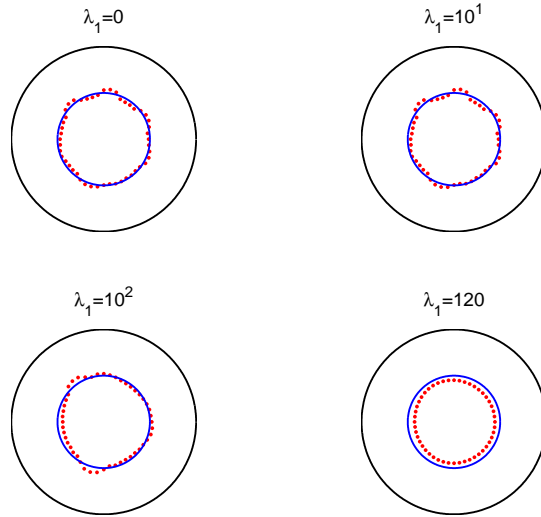


FIGURE 3. Example 1: Results after 1000 iterations for noise $p = 10\%$ and regularization with λ_1 .

5.2. **Example 2.** In this example, we consider a more complicated peanut-shaped rigid inclusion whose boundary $\partial\Omega_1$ is described by the radial parametrization

$$r(\vartheta) = \frac{3}{4} \sqrt{\cos^2(\vartheta) + 0.25 \sin^2(\vartheta)}, \quad \vartheta \in [0, 2\pi), \quad (5.4)$$

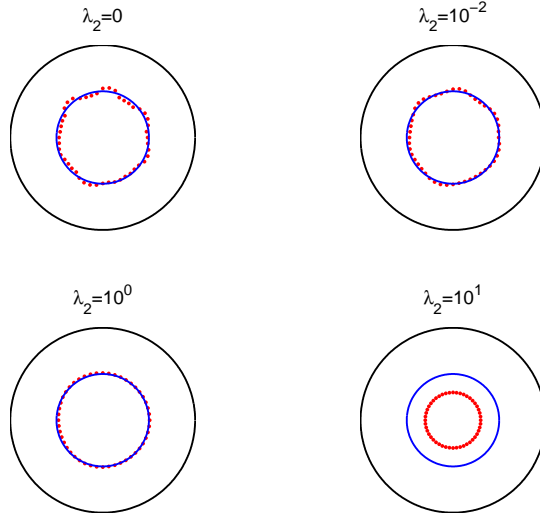


FIGURE 4. Example 1: Results after 1000 iterations for noise $p = 10\%$ and regularization with λ_2 .

in the case of $\alpha = 1$, which was considered in [25]. The Dirichlet data (2.1b) on $\partial\Omega_2$ is taken as [25]

$$u(1, \vartheta) = f(\vartheta) = e^{-\cos^2 \vartheta}, \quad \vartheta \in [0, 2\pi]. \quad (5.5)$$

Since in this case no analytical solution is available, the Neumann data (2.1d) is simulated by solving the direct well-posed problem (2.1a), (2.1c) and (5.5), when $\partial\Omega_1$ is given by (5.4), using the direct TCM with $M_1 = M_2 = 100$, $N = 30$. In order to avoid committing an inverse crime, the inverse solver is applied using $M_1 = M_2 = 64$, $N = 6$.

In Figure 5 we present typical examples of reconstructed curves with noise $p = 10\%$ with no regularization for different numbers of iterations. In Figures 6 and 7 we present the corresponding reconstructed curves with $p = 10\%$, after 1000 iterations and various regularization parameters λ_1 with $\lambda_2 = 0$, and λ_2 with $\lambda_1 = 0$, respectively. The L-curves [21, 20] obtained with regularization in λ_1 or λ_2 for noise $p = 10\%$ and 1000 iterations are presented in Figures 8(a) and (b), respectively. From Figure 5 it can be seen that the numerically retrieved shapes are stable and in reasonable agreement with the exact shape (5.4). This is somewhat surprising since no regularization has been imposed, but it may be that oscillations will start to appear only after a larger number of iterations than 1000. Furthermore, Figure 6 shows that regularization with λ_1 produces almost no improvement and, in fact, Figure 8(a) illustrates that an L-curve could not be obtained in this case. On the other hand, Figure 7 shows that regularization with λ_2 between 10^{-2} to 1 does produce smoother and more stable and accurate solutions with the choice of the regularization parameter given by the corner of the L-curve illustrated in Figure 8(b).

5.3. Example 3. In this example, we again consider the peanut-shaped cavity whose boundary $\partial\Omega_1$ is described by the radial parametrization (5.4), this time in the case of $\alpha = 0$, which was studied in [25, 29]. As in Example 2, the Dirichlet data (2.1b) on $\partial\Omega_2$ is given by (5.5). The Neumann data (2.1d) is simulated by solving the direct problem using the direct TCM with, $M_1 = M_2 = 100$, $N = 28$. In order to avoid committing an inverse crime, the inverse solver is applied using $M_1 = M_2 = 64$, $N = 5$.

In Figure 9 we present typical examples of reconstructed curves with noise level of $p = 5\%$ with no regularization for different numbers of iterations. In Figures 10 and 11 we present the corresponding reconstructed curves with $p = 5\%$, after 500 iterations and various regularization parameters λ_1 with $\lambda_2 = 0$, and λ_2 with $\lambda_1 = 0$, respectively.

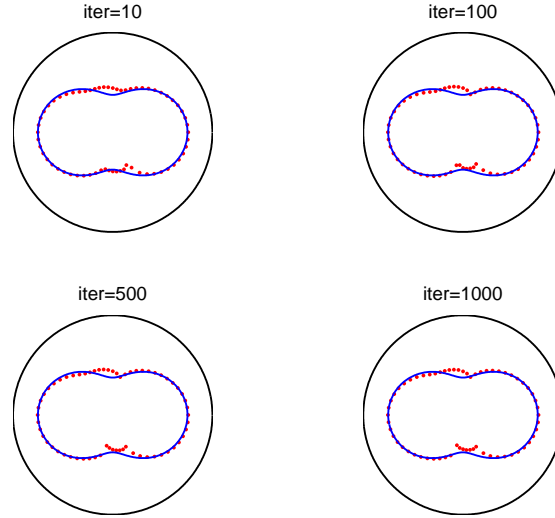


FIGURE 5. Example 2: Results for noise $p = 10\%$, no regularization and various numbers of iterations.

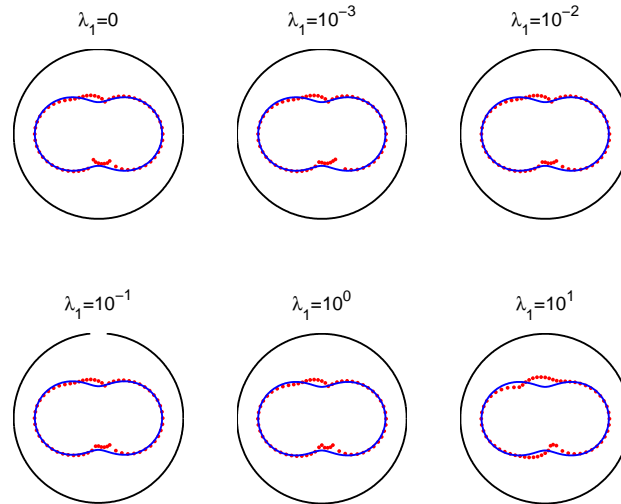


FIGURE 6. Example 2: Results after 1000 iterations for noise $p = 10\%$ and regularization with λ_1 .

When $\lambda_2 \neq 0$, it was observed that in some cases the iterative process converged in fewer than the prescribed 500 iterations. From Figures 9-11 the same conclusions as those drawn from Figures 5-7 are obtained, although the reconstructions of the cavity in Example 3 are slightly less accurate than the reconstructions of the rigid inclusion in Example 2.

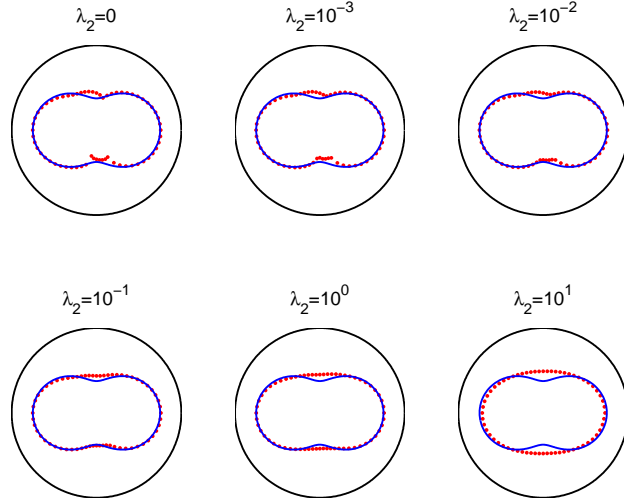


FIGURE 7. Example 2: Results after 1000 iterations for noise $p = 10\%$ and regularization with λ_2 .

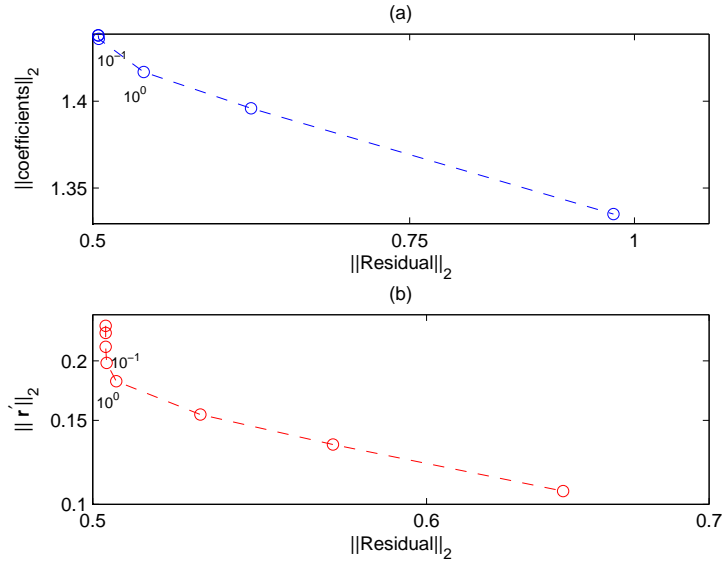


FIGURE 8. Example 2: L-curves obtained with regularization in (a) λ_1 and (b) λ_2 for noise $p = 10\%$.

5.4. **Example 4.** We consider a rigid inclusion Ω_1 , i.e. $\alpha = 1$, described by $X = 0.5, Y = -1, R = 3.5$ and the radial parametrization

$$r(\vartheta) = 1.52 - 0.24 \sin(3\vartheta), \quad \vartheta \in [0, 2\pi). \quad (5.6)$$

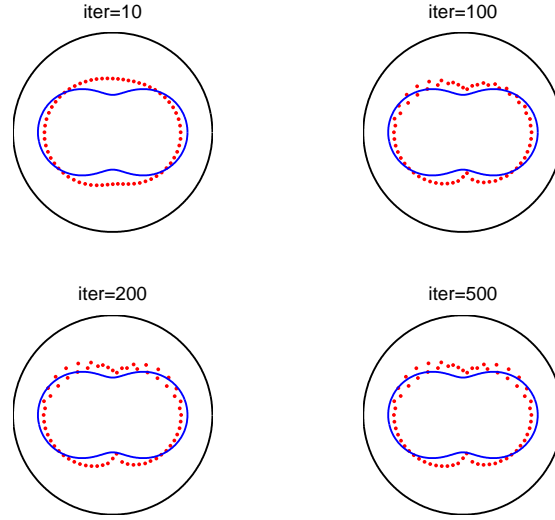


FIGURE 9. Example 3: Results for noise $p = 5\%$ and no regularization.

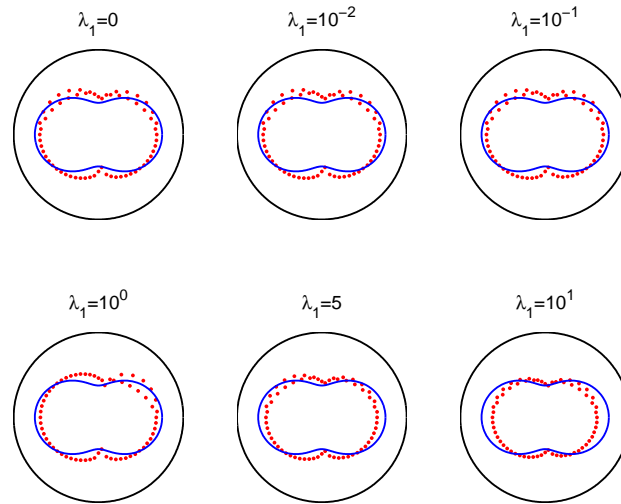


FIGURE 10. Example 3: Results for noise $p = 5\%$ and regularization with λ_1 .

This example, which was considered in [44] for the Stokes equations in slow viscous flow and in [30], is more difficult than the previous examples because of the fact that we now consider the centre of the cavity as unknown. The Neumann data (2.1d) is simulated by solving the direct problem using the MFS with 400 sources and 400

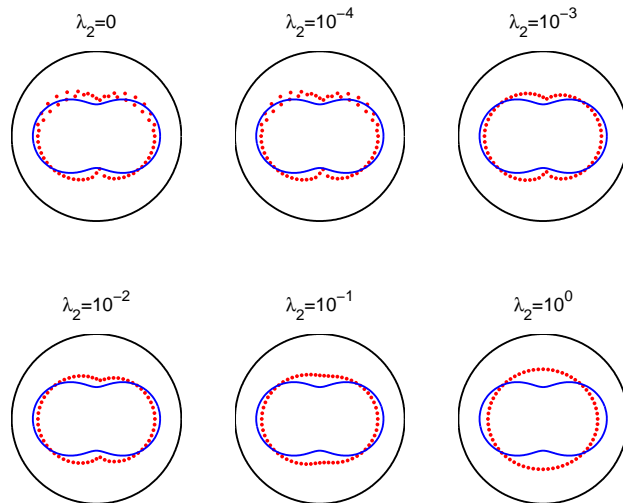


FIGURE 11. Example 3: Results for noise $p = 5\%$ and regularization with λ_2 .

collocation points. The inverse TCM solver is applied using $M_1 = M_2 = 64, N = 6$. The starting position of the centre in the iterative process was taken to be the origin.

In Figure 12 we present typical examples of reconstructed curves with noise level of $p = 5\%$ with no regularization for different numbers of iterations. In Figures 13 and 14 we present the corresponding reconstructed curves with $p = 5\%$, after 1000 iterations and various regularization parameters λ_1 with $\lambda_2 = 0$, and λ_2 with $\lambda_1 = 0$, respectively. From Figures 12-14, the same conclusions as those drawn from Figures 5-7 for Example 2 and Figures 9-11 for Example 3 are obtained. This shows that the reconstruction method also performs well when the centre of the star-shaped void is unknown.

5.5. Example 5. We finally consider the same obstacle as in Example 4, given by (5.6) but in the case of $\alpha = 0$, i.e. Ω_1 is a cavity. The numerical details are the same as in Example 4.

In Figure 15 we present the results obtained for different numbers of iterations, with $p = 5\%$ noise and no regularization. In Figures 16 and 17 we present the corresponding reconstructed curves with $p = 5\%$, after 500 iterations and various regularization parameters λ_1 with $\lambda_2 = 0$, and λ_2 with $\lambda_1 = 0$, respectively. From Figures 15 and 16 it can be seen that the numerically obtained shapes with $\lambda_1 = \lambda_2 = 0$, or $\lambda_2 = 0, \lambda_1 > 0$, are unstable, whilst from Figure 17 it can be observed that regularization with λ_2 between 10^{-4} and 10^{-2} produces smoother stable reconstructions.

6. EXTENSION TO MULTIPLE VOIDS

The TCM analysis performed so far showed the successful implementation of this method for the identification of a single void. In this section we extend the analysis to multiple voids which may contain both cavities and rigid inclusions. For the sake of clarity, we describe the formulation for the case of two voids. Therefore, we consider the inverse problem

$$\Delta u = 0 \quad \text{in } \Omega, \quad (6.1a)$$

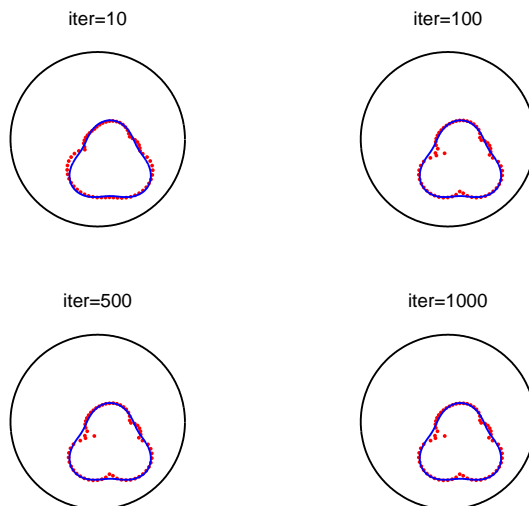


FIGURE 12. Example 4: Results for noise $p = 5\%$, no regularization and various numbers of iterations.

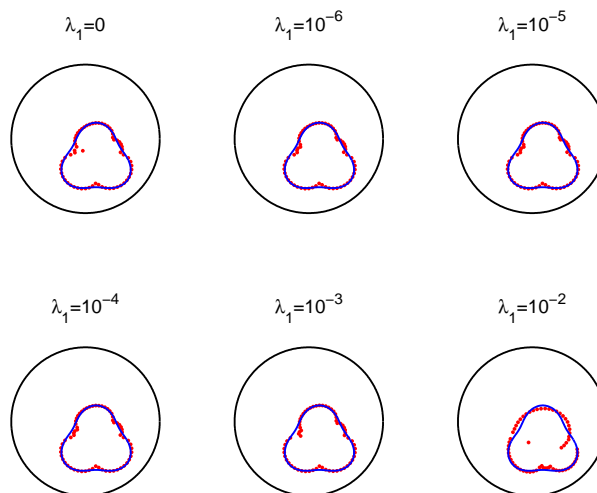


FIGURE 13. Example 4: Results after 1000 iterations for noise $p = 5\%$ and regularization with λ_1 .

subject to the boundary conditions

$$u = f \quad \text{and} \quad \partial_n u = g \quad \text{on} \quad \partial\Omega_2, \quad (6.1b)$$

and the homogeneous boundary conditions

$$\alpha_1 u + (1 - \alpha_1) \partial_n u = 0 \quad \text{on} \quad \partial\Omega_1^a, \quad \text{where} \quad \alpha_1 \in \{0, 1\}, \quad (6.1c)$$

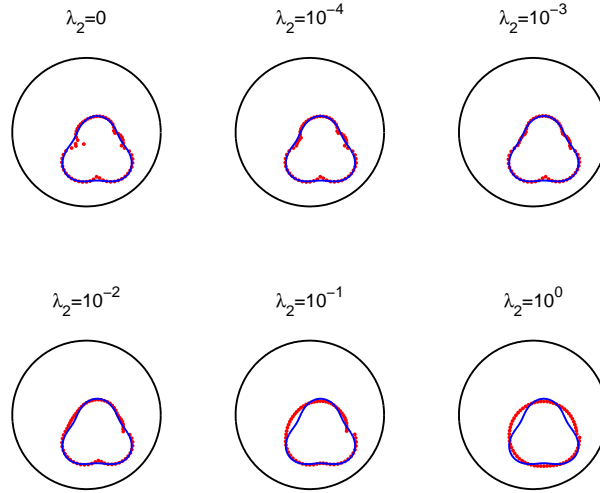


FIGURE 14. Example 4: Results after 1000 iterations for noise $p = 5\%$ and regularization with λ_2 .

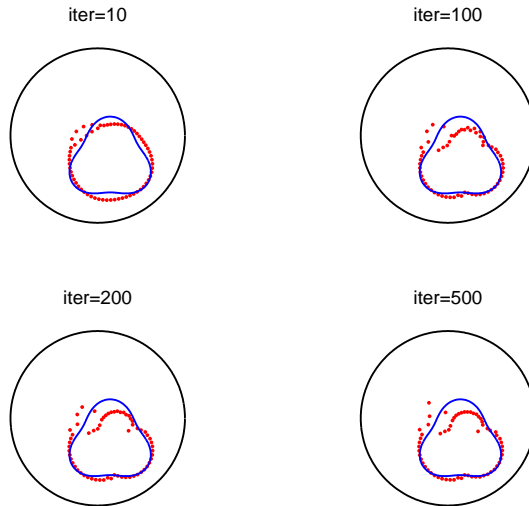


FIGURE 15. Example 5: Results for noise $p = 5\%$, no regularization and various numbers of iterations.

and

$$\alpha_2 u + (1 - \alpha_2) \partial_n u = 0 \quad \text{on} \quad \partial\Omega_1^b, \quad \text{where} \quad \alpha_2 \in \{0, 1\}. \quad (6.1d)$$

Here Ω_1^a and Ω_1^b are two disjoint voids, such that $\Omega_1^a \cup \Omega_1^b = \Omega_1$ and $\overline{\Omega_1^a} \cap \overline{\Omega_1^b} = \emptyset$.

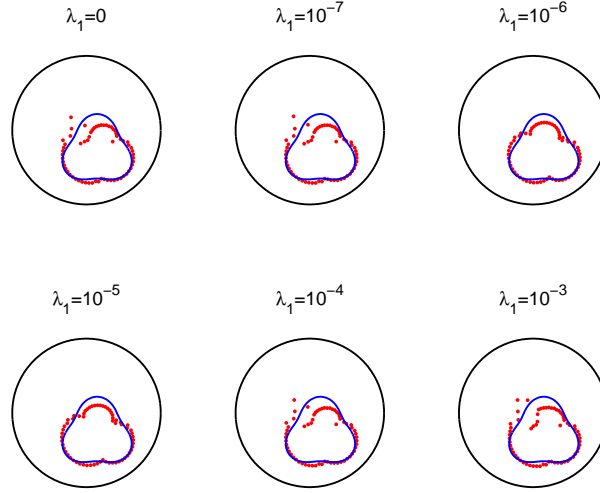


FIGURE 16. Example 5: Results after 500 iterations for noise $p = 5\%$ and regularization with λ_1 .

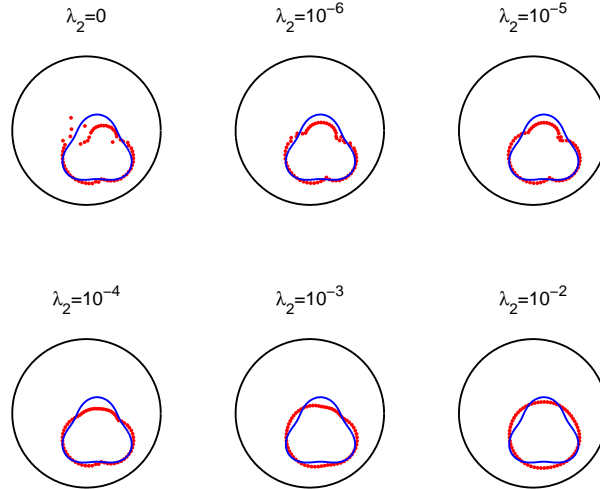


FIGURE 17. Example 5: Results after 500 iterations for noise $p = 5\%$ and regularization with λ_2 .

The outer boundary collocation points are chosen as

$$\mathbf{x}_{M_1+M_2+\ell} = R(\cos \tilde{\vartheta}_\ell, \sin \tilde{\vartheta}_\ell), \quad \ell = \overline{1, M_3}, \quad (6.2)$$

where $\tilde{\vartheta}_\ell = \frac{2\pi(\ell-1)}{M_3}$, $\ell = \overline{1, M_3}$.

We further assume that the unknown boundaries $\partial\Omega_1^a$ and $\partial\Omega_1^b$ are a smooth, star-like curves with respect to their centres which have *unknown* coordinates (X^a, Y^a) and (X^b, Y^b) , respectively. This means that their equations in polar coordinates can be written as

$$x = X^a + r^a(\vartheta) \cos \vartheta, \quad y = Y^a + r^a(\vartheta) \sin \vartheta, \quad (6.3)$$

$$x = X^b + r^b(\vartheta) \cos \vartheta, \quad y = Y^b + r^b(\vartheta) \sin \vartheta, \quad \vartheta \in [0, 2\pi), \quad (6.4)$$

where r^a and r^b are smooth 2π -periodic functions.

The discretized forms of (6.3) and (6.4) for $\partial\Omega_1^a$ and $\partial\Omega_1^b$ become

$$r_k^a = r^a(\vartheta_k), \quad k = \overline{1, M_1} \quad \text{and} \quad r_\ell^b = r^b(\vartheta_\ell) \quad \ell = \overline{1, M_2}. \quad (6.5)$$

We choose the inner boundary collocation points as

$$\mathbf{x}_k = (X^a, Y^a) + r_k^a (\cos \vartheta_k, \sin \vartheta_k), \quad k = \overline{1, M_1} \quad (6.6)$$

$$\mathbf{x}_k = (X^b, Y^a) + r_k^b (\cos \vartheta_k, \sin \vartheta_k), \quad k = \overline{M_1 + 1, M_1 + M_2}. \quad (6.7)$$

Since we have more than one void and their centres are not at the origin, the basis (3.2) needs to be modified as in the doubly connected domain, to (see [16])

$$\begin{aligned} & \{1, \log |z - z^a|, \log |z - z^b|, \Re(z^n), \Im(z^n), \Re((z - z^a)^{-n}), \Im((z - z^a)^{-n}), \\ & \Re((z - z^b)^{-n}), \Im((z - z^b)^{-n}); z = x + iy, n \in \mathbb{N}\}, \end{aligned} \quad (6.8)$$

where $z^a = X^a + iY^a$, $z^b = X^b + iY^b$ and therefore the TCM approximation becomes

$$\begin{aligned} u_N(\boldsymbol{\alpha}, \boldsymbol{\beta}, \boldsymbol{\gamma}^a, \boldsymbol{\gamma}^b, \boldsymbol{\delta}^a, \boldsymbol{\delta}^b; \mathbf{x}) &= \alpha_0 + \gamma_0^a \log |z - z^a| + \gamma_0^b \log |z - z^b| + \sum_{k=1}^N \alpha_k \Re \{z^k\} + \sum_{k=1}^N \beta_k \Im \{z^k\} \\ &+ \sum_{k=1}^N \gamma_k^a \Re \{(z - z^a)^{-k}\} + \sum_{k=1}^N \delta_k^a \Im \{(z - z^a)^{-k}\} + \sum_{k=1}^N \gamma_k^b \Re \{(z - z^b)^{-k}\} + \sum_{k=1}^N \delta_k^b \Im \{(z - z^b)^{-k}\}, \end{aligned} \quad (6.9)$$

for $\mathbf{x} = (x, y) \in \overline{\Omega}$.

The coefficients $(\alpha_k)_{k=\overline{0, N}}$, $(\beta_k)_{k=\overline{1, N}}$, $(\gamma_k^\ell)_{k=\overline{0, N}, \ell=a, b}$, $(\delta_k^\ell)_{k=\overline{1, N}, \ell=a, b}$ in (6.9), the radii $(r_k^a)_{k=\overline{1, M_1}}$, $(r_k^b)_{k=\overline{1, M_2}}$ in (6.5), and the coordinates of the centres (X^a, Y^a) , (X^b, Y^b) can be determined by imposing the boundary conditions in a least-squares sense. This leads to the minimization of the functional

$$\begin{aligned} S(\boldsymbol{\alpha}, \boldsymbol{\beta}, \boldsymbol{\gamma}^a, \boldsymbol{\gamma}^b, \boldsymbol{\delta}^a, \boldsymbol{\delta}^b, \mathbf{r}^a, \mathbf{r}^b, \mathbf{C}) &:= \sum_{j=M_1+M_2+1}^{M_1+M_2+M_3} \left[u_N(\boldsymbol{\alpha}, \boldsymbol{\beta}, \boldsymbol{\gamma}^a, \boldsymbol{\gamma}^b, \boldsymbol{\delta}^a, \boldsymbol{\delta}^b; \mathbf{x}_j) - f(\mathbf{x}_j) \right]^2 \\ &+ \sum_{j=M_1+M_2+1}^{M_1+M_2+M_3} \left[\partial_n u_N(\boldsymbol{\alpha}, \boldsymbol{\beta}, \boldsymbol{\gamma}^a, \boldsymbol{\gamma}^b, \boldsymbol{\delta}^a, \boldsymbol{\delta}^b; \mathbf{x}_j) - g^\varepsilon(\mathbf{x}_j) \right]^2 \\ &+ \sum_{j=1}^{M_1} \left[\alpha_1 u_N(\boldsymbol{\alpha}, \boldsymbol{\beta}, \boldsymbol{\gamma}^a, \boldsymbol{\gamma}^b, \boldsymbol{\delta}^a, \boldsymbol{\delta}^b; \mathbf{x}_j) + (1 - \alpha_1) \partial_n u_N(\boldsymbol{\alpha}, \boldsymbol{\beta}, \boldsymbol{\gamma}^a, \boldsymbol{\gamma}^b, \boldsymbol{\delta}^a, \boldsymbol{\delta}^b; \mathbf{x}_j) \right]^2 \\ &+ \sum_{j=M_1+1}^{M_1+M_2} \left[\alpha_2 u_N(\boldsymbol{\alpha}, \boldsymbol{\beta}, \boldsymbol{\gamma}^a, \boldsymbol{\gamma}^b, \boldsymbol{\delta}^a, \boldsymbol{\delta}^b; \mathbf{x}_j) + (1 - \alpha_2) \partial_n u_N(\boldsymbol{\alpha}, \boldsymbol{\beta}, \boldsymbol{\gamma}^a, \boldsymbol{\gamma}^b, \boldsymbol{\delta}^a, \boldsymbol{\delta}^b; \mathbf{x}_j) \right]^2 \\ &+ \lambda_1 \left(|\boldsymbol{\alpha}|^2 + |\boldsymbol{\beta}|^2 + |\boldsymbol{\gamma}^a|^2 + |\boldsymbol{\gamma}^b|^2 + |\boldsymbol{\delta}^a|^2 + |\boldsymbol{\delta}^b|^2 \right) + \lambda_2^a \sum_{\ell=2}^{M_1} (r_\ell^a - r_{\ell-1}^a)^2 + \lambda_2^b \sum_{\ell=2}^{M_2} (r_\ell^b - r_{\ell-1}^b)^2, \end{aligned} \quad (6.10)$$

where $\lambda_1, \lambda_2^a, \lambda_2^b \geq 0$ are regularization parameters to be prescribed, $\mathbf{r}^a = [r_1^a, r_2^a, \dots, r_N^a]^T$, $\mathbf{r}^b = [r_1^b, r_2^b, \dots, r_N^b]^T$, and $\mathbf{C} = [X^a, Y^a, X^b, Y^b]^T$. The number of unknowns is $6N + 3 + M_1 + M_2 + 4$ and the number of boundary collocation equations $M_1 + M_2 + 2M_3$, and thus we need to take $2M_3 \geq 6N + 7$.

6.1. Example 6. We consider the case when two rigid inclusions $\alpha_1 = \alpha_2 = 1$) Ω_1^a and Ω_1^b are present. The domain Ω_1^a is a disk of radius 1, with centre $X^a = 1, Y^a = -1$, while the domain Ω_1^b is described by the radial parametrization

$$r(\vartheta) = \frac{1 + 0.8 \cos(\vartheta) + 0.2 \sin(2\vartheta)}{1 + 0.7 \cos(\vartheta)}, \quad \vartheta \in [0, 2\pi), \quad (6.11)$$

and has centre $X^b = -1, Y^b = 1$. In this example which was also examined in [29] we take $R = 3.5$. The Neumann data (2.1d) is simulated by solving the direct problem using the MFS with 600 singularities and 600 collocation points. The inverse TCM solver is applied using $M_1 = M_2 = 32, M_3 = 64, N = 6$. The starting position of the centres in the iterative process was taken to be $(0.5, -0.5)$ and $(-0.5, 0.5)$, respectively.

In Figure 18 we present the results obtained for different numbers of iterations, no regularization, and $p = 5\%$ noise. In Figures 19 and 20 we present the corresponding reconstructed curves with $p = 5\%$ noise, after 500 iterations, and various levels of regularization λ_1 with $\lambda_2 = \lambda_2^a = \lambda_2^b = 0$, and $\lambda_1 = 0$ with $\lambda_2 = \lambda_2^a = \lambda_2^b$, respectively. Overall, Figures 18-20 illustrate that the MFS can successfully retrieve voids having two connected components.

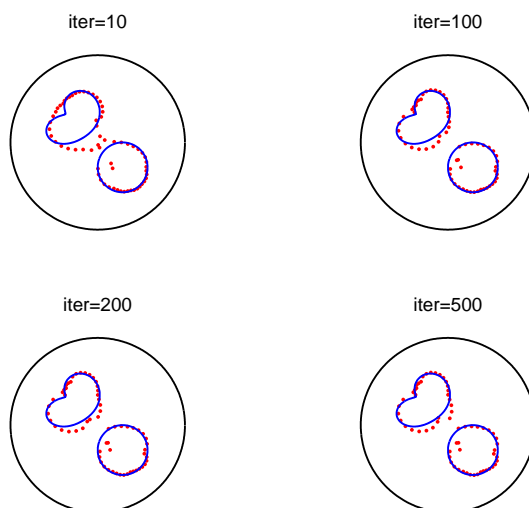


FIGURE 18. Example 6: Results for noise $p = 5\%$, no regularization and various numbers of iterations.

7. CONCLUSIONS

We have applied the TCM combined with a nonlinear least-squares minimization for the solution of several inverse geometric problems including the detection of voids such as rigid inclusions and cavities. The centre of the assumed star-shaped void may or may not be known. For several test examples involving various shapes the method performed well producing accurate and stable reconstructions with relatively few terms in the approximating expansion of the solution. In some of the cases where cavities were considered ill-conditioning was observed. This is due to the inherent ill-conditioning of the TCM. Regularization appears to alleviate to a great extent this problem. The reconstruction of multiple voids is also possible with the proposed method. Extensions of the present approach could include applications to inverse geometric problems governed by the Helmholtz and biharmonic equations as

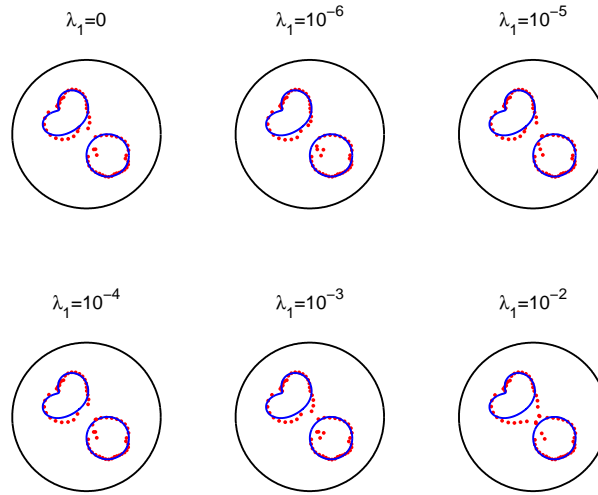


FIGURE 19. Example 6: Results after 500 iterations for noise $p = 5\%$ and regularization with λ_1 .

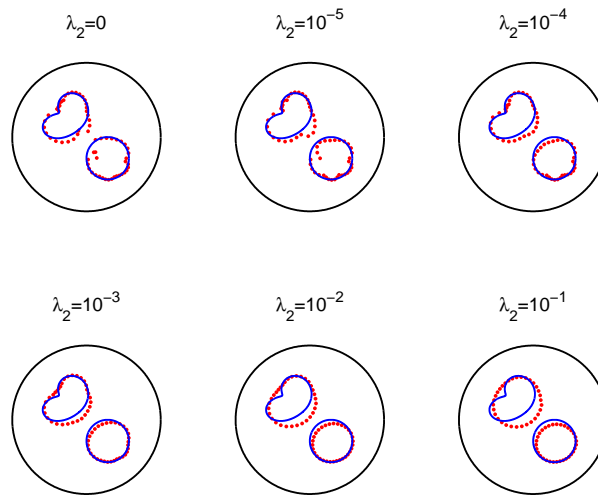


FIGURE 20. Example 6: Results after 500 iterations for noise $p = 5\%$ and regularization with λ_2 .

well as applications to three-dimensional inverse geometric problems by using the appropriate bases listed in [38, pages 32-33].

ACKNOWLEDGEMENTS

The authors wish to thank Professor Nick Papamichael for many enlightening discussions and are also grateful to the University of Cyprus for supporting this research. L. Marin also acknowledges the financial support received from the Romanian National Authority for Scientific Research, CNCS-UEFISCDI, project number PN-II-ID-PCE-2011-3-0521.

REFERENCES

- [1] D. Borman, D. B. Ingham, B. T. Johansson, and D. Lesnic, *The method of fundamental solutions for detection of cavities in EIT*, J. Integral Equations Appl. **21** (2009), 381–404.
- [2] H.-F. Chan, *Meshless Method and Exponentially Convergent Scalar Homotopy Algorithm for the Inverse Boundary Determination Problem*, Master's thesis, Department of Harbor and River Engineering, National Taiwan Ocean University, Keelung, Taiwan, 2011.
- [3] H.-F. Chan, C.-M. Fan, and W. Yeih, *Solution of inverse boundary optimization problem by Trefftz method and exponentially convergent scalar homotopy algorithm*, CMC Comput. Mater. Continua **24** (2011), 125–142.
- [4] J.-T. Chen, Y.-T. Lee, S.-R. Yu, and S.-C. Shieh, *Equivalence between the Trefftz method and the method of fundamental solution for the annular Green's function using the addition theorem and image concept*, Eng. Anal. Bound. Elem. **33** (2009), 678–688.
- [5] J.-T. Chen, C.-S. Wu, Y.-T. Lee, and K.-H. Chen, *On the equivalence of the Trefftz method and method of fundamental solutions for Laplace and biharmonic equations*, Comput. Math. Appl. **53** (2007), 851–879.
- [6] C.-H. Cheng and M.-H. Chang, *A simplified conjugate-gradient method for shape identification based on thermal data*, Num. Heat Transfer, Part B **43** (2003), 489–507.
- [7] M. Ciałkowski and K. Grysa, *Trefftz method in solving the inverse problems*, J. Inverse Ill-Posed Probl. **18** (2010), 595–616.
- [8] M. J. Ciałkowski and Frąckowiak, *Solution of the stationary 2D inverse heat conduction problem by Trefftz method*, J. Thermal Science **11** (2002), 148–162.
- [9] M. J. Ciałkowski, A. Frąckowiak, and K. Grysa, *Physical regularization for inverse problems of stationary heat conduction*, J. Inverse Ill-Posed Probl. **15** (2007), 347–364.
- [10] ———, *Solution of a stationary inverse heat conduction problem by means of Trefftz non-continuous method*, Int. J. Heat Mass Transfer **50** (2007), 2170–2181.
- [11] T. F. Coleman and Y. Li, *On the convergence of interior-reflective Newton methods for nonlinear minimization subject to bounds*, Math. Programming **67** (1994), 189–224.
- [12] ———, *An interior trust region approach for nonlinear minimization subject to bounds*, SIAM J. Optim. **6** (1996), 418–445.
- [13] S. Das and A. K. Mitra, *An algorithm for the solution of inverse Laplace problems and its application in flaw identification in materials*, J. Comput. Phys. **99** (1992), 99–105.
- [14] C.-M. Fan and H.-F. Chan, *Modified collocation Trefftz method for the geometry boundary identification problem of heat conduction*, Numerical Heat Transfer, Part B **59** (2011), 58–75.
- [15] C.-M. Fan, H.-F. Chan, C.-L. Kuo, and W. Yeih, *Numerical solutions of boundary detection problems using modified collocation Trefftz method and exponentially convergent scalar homotopy algorithm*, Eng. Anal. Bound. Elem. **36** (2012), 2–8.
- [16] D. Gaier, *Konstruktive Methoden der Konformen Abbildung*, Springer Tracts in Natural Philosophy, Vol. 3, Springer-Verlag, Berlin, 1964.
- [17] R. Gallego and J. Suarez, *Solution of inverse problems by boundary integral equations without residual minimization*, Int. J. Solids Struct. **37** (2000), 5629–5652.
- [18] J. Hadamard, *Lectures on Cauchy Problem in Linear Partial Differential Equations*, Yale University Press, New Haven, 1923.
- [19] H. Haddar and R. Kress, *Conformal mappings and inverse boundary value problems*, Inverse Problems **21** (2005), 935–953.
- [20] P. C. Hansen, *Discrete Inverse Problems: Insight and Algorithms*, SIAM, Philadelphia, 2010.
- [21] P. C. Hansen and D. P. O'Leary, *The use of the L-curve in the regularization of discrete ill-posed problems*, SIAM J. Sci. Comput. **14** (1993), 1487–1503.
- [22] I. Herrera, *Boundary Methods: an Algebraic Theory*, Applicable Mathematics Series, Pitman (Advanced Publishing Program), Boston, MA, 1984.
- [23] I. Herrera and F. J. Sabina, *Connectivity as an alternative to boundary integral equations: construction of bases*, Proc. Nat. Acad. Sci. U.S.A. **75** (1978), 2059–2063.
- [24] C.-H. Huang and T.-Y. Hsiung, *An inverse design problem of estimating optimal shape of cooling passages in turbine blades*, Int. J. Heat Mass Transfer **42** (1999), 4307–4319.
- [25] O. Ivanyshyn and R. Kress, *Nonlinear integral equations for solving inverse boundary value problems for inclusions and cracks*, J. Integral Equations Appl. **18** (2006), 13–38.
- [26] J. Jirousek and A. P. Zieliński, *Survey of Trefftz-type element formulations*, Comput. & Structures **63** (1997), 225–242.
- [27] A. Karageorghis and D. Lesnic, *Detection of cavities using the method of fundamental solutions*, Inverse Probl. Sci. Eng. **17** (2009), 803–820.

- [28] ———, *The method of fundamental solutions for the inverse conductivity problem*, Inverse Probl. Sci. Eng. **18** (2010), 567–583.
- [29] A. Karageorghis, D. Lesnic, and L. Marin, *A moving pseudo-boundary MFS for void detection*, Numer. Methods Partial Differential Equations, to appear, <http://dx.doi.org/10.1002/num.21739>.
- [30] ———, *A survey of applications of the MFS to inverse problems*, Inverse Probl. Sci. Eng. **19** (2011), 309–336.
- [31] M. S. Karaš and A. P. Zieliński, *Boundary-value recovery by the Trefftz approach in structural inverse problems*, Comm. Numer. Methods Engrg. **24** (2008), 605–625.
- [32] A. J. Kassab and J. E. Pollard, *Automated algorithm for high the nondestructive detection of subsurface cavities by the IR-CAT method*, J. Nondestructive Evaluation **12** (1993), 175–186.
- [33] A. J. Kassab and J. E. Pollard, *Cubic spline anchored grid pattern algorithm for high resolution detection of subsurface cavities by the IR-CAT method*, Num. Heat Transfer, Part B **26** (1994), 63–71.
- [34] A. J. Kassab, E. A. Divo, and F. Rodriguez, *An efficient superposition technique for cavity detection and shape optimization*, Num. Heat Transfer, Part B **46** (2004), 1–30.
- [35] M. J. Kazemzadeh-Parsi and F. Daneshmand, *Solution of geometric inverse heat conduction problems by smoothed fixed grid finite element method*, Finite Elem. Anal. Design **45**, (2009), 599–611.
- [36] E. Kita and N. Kamiya, *Trefftz method: an overview*, Adv. Eng. Software **24** (1995), 3–12.
- [37] C. A. Kokkinos, N. Papamichael, and A. B. Sideridis, *An orthonormalization method for the approximate conformal mapping of multiply-connected domains*, IMA J. Numer. Anal. **10** (1990), 343–359.
- [38] J. A. Kołodziej and A. P. Zieliński, *Boundary Collocation Techniques and their Application in Engineering*, WIT Press, Southampton, 2009.
- [39] V. M. A. Leitão, *Applications of multi-region Trefftz-collocation to fracture mechanics*, Eng. Anal. Bound. Elem. **22** (1998), 251–256.
- [40] Z.-C. Li, T.-T. Lu, H.-T. Huang, and A. H.-D. Cheng, *Trefftz, collocation, and other boundary methods—a comparison*, Numer. Methods Partial Differential Equations **23** (2007), 93–144.
- [41] C.-S. Liu, *An effectively modified direct Trefftz method 2d potential problems considering the domain’s characteristic length*, Eng. Anal. Bound. Elem. **31** (2007), 983–993.
- [42] ———, *A highly accurate collocation Trefftz method for solving the Laplace equation in the doubly connected domains*, Numer. Methods Partial Differential Equations **24** (2008), 179–192.
- [43] ———, *A modified collocation Trefftz method for the inverse Cauchy problem of Laplace equation*, Eng. Anal. Bound. Elem. **32** (2008), 778–785.
- [44] N. F. M. Martins and A. L. Silvestre, *An iterative MFS approach for the detection of immersed obstacles*, Eng. Anal. Bound. Elem. **32** (2008), 517–524.
- [45] The MathWorks, Inc., 3 Apple Hill Dr., Natick, MA, *Matlab*.
- [46] N. S. Mera, L. Elliott, and D. B. Ingham, *Detection of subsurface cavities in IR-CAT by a real coded genetic algorithm*, Applied Soft Comput. **2** (2002), 129–139.
- [47] N. S. Mera, *Efficient optimization processes using kriging approximation models in electrical impedance tomography*, Int. J. Numer. Meth. Engrg. **69** (2007), 202–220.
- [48] A. G. Ramm, *A geometrical inverse problem*, Inverse Problems **2** (1986), L19–L21.
- [49] T. Shigeta and D. L. Young, *Mathematical and numerical studies on meshless methods for exterior unbounded domain problems*, J. Comput. Phys. **230** (2011), 6900–6915.
- [50] J. Y. Tan, J. M. Zhao, and L. H. Liu, *Meshless method for geometry boundary identification problem of heat conduction*, Num. Heat Transfer, Part B **55** (2009), 135–154.
- [51] E. Trefftz, *Ein Gegenstück zum Ritzschen Verfahren*, 2^{er} Intern. Kongr. für Techn. Mech., Zürich, 1926, pp. 131–137.
- [52] C.-C. Tsai and P.-H. Lin, *A multiple-precision study on the modified collocation Trefftz method*, CMC Comput. Mater. Continua **28** (2012), 231–259.
- [53] W.-J. Yan and Y.-C. Ma, *Numerical simulation for the shape reconstruction of a cavity*, Numer. Methods Partial Differential Equations **25** (2009), 460–469.
- [54] W. Yeih, C.-S. Liu, C.-L. Kuo, and S. N. Atluri, *On solving the direct/inverse Cauchy problems of Laplace equation in a multiply connected domain, using the generalized multiple-source-point boundary-collocation Trefftz method and characteristic lengths*, CMC Comput. Mater. Continua **17** (2010), 275–302.
- [55] A. P. Zieliński, *On trial functions applied in the generalized Trefftz method*, Adv. Eng. Software **24** (1995), 147–155.
- [56] ———, *Special Trefftz elements and improvement of their conditioning*, Commun. Numer. Methods Engrg. **13** (1997), 765–775.

DEPARTMENT OF MATHEMATICS AND STATISTICS, UNIVERSITY OF CYPRUS/ ΠΑΝΕΠΙΣΤΗΜΙΟ ΚΥΠΡΟΥ, P.O.Box 20537, 1678 NICOSIA/ΛΕΥΚΩΣΙΑ,
CYPRUS/ΚΥΠΡΟΣ

E-mail address: andreask@ucy.ac.cy

DEPARTMENT OF APPLIED MATHEMATICS, UNIVERSITY OF LEEDS, LEEDS LS2 9JT, UK

E-mail address: amt51d@maths.leeds.ac.uk

INSTITUTE OF SOLID MECHANICS, ROMANIAN ACADEMY, 15 CONSTANTIN MILLE, 010141 BUCHAREST, AND CENTRE FOR CONTINUUM
MECHANICS, FACULTY OF MATHEMATICS AND COMPUTER SCIENCE, UNIVERSITY OF BUCHAREST, 14 ACADEMIEI, 010014 BUCHAREST,
ROMANIA

E-mail address: marin.liviu@gmail.com; liviu@imsar.bu.edu.ro